Quantum Electronics **39** (9) 869 – 878 (2009)

LASER APPLICATIONS AND OTHER TOPICS IN QUANTUM ELECTRONICS

PACS numbers: 42.55.Px; 42.62.Fi; 07.07.Df
DOI: 10.1070/QE2009v039n09ABEH014044

Measurements of gas parameters in plasma-assisted supersonic combustion processes using diode laser spectroscopy

M.A. Bolshov, Yu.A. Kuritsyn, V.V. Liger, V.R. Mironenko, S.B. Leonov, D.A. Yarantsev

***Abstract*. We report a procedure for temperature and water vapour concentration measurements in an unsteady-state combustion zone using diode laser absorption spectroscopy. The procedure involves measurements of the absorption spectrum of water molecules around 1.39 μm. It has been used to determine hydrogen combustion parameters in $M = 2$ gas flows in the test section of a supersonic wind tunnel. The relatively high intensities of the absorption lines used have enabled direct absorption measurements. We describe a differential technique for measurements of transient absorption spectra, the procedure we used for primary data processing and approaches for determining the gas temperature and H_2O concentration in the probed zone. The measured absorption spectra are fitted with spectra simulated using parameters from spectroscopic databases. The combustion-time-averaged (~ 50 ms) gas temperature and water vapour partial pressure in the hot wake region are determined to be 1050 K and 21 Torr, respectively. The large signal-to-noise ratio in our measurements allowed us to assess the temporal behaviour of these parameters. The accuracy in our temperature measurements in the probed zone is ~ 40 K.**

Keywords: *absorption spectroscopy, diode laser, probing of gas flows, temperature and concentration measurements.*

1. Introduction

Diode laser absorption spectroscopy (DLAS) is widely used to probe processes in flames and multicomponent gas flows [1]. This technique has a number of important advantages over emission and fluorescence spectroscopies. DLAS does not require large radiation collection angles: all the information about the absorbing object is carried by the narrow, weakly diverging laser beam transmitted by the probed medium. Therefore, the influence of the intrinsic emission from hot gas and the nonselective scattering of the laser beam, which pose serious problems in the emission and fluorescence techniques, can be almost completely suppressed via spatial filtration of the laser beam incident on the detector. This allows one to substantially reduce the background level and to probe even the hottest, and the most emissive, zones of the object of interest.

When a gas mixture is sensed, the DLAS technique probes absorbing species (atoms or simple molecules) that have sufficiently narrow lines. As a rule, one can select either isolated absorption lines or lines that overlap only weakly. Test molecules are either those naturally forming in the probed volume or tracers added to the target gas [1, 2]. There are a number of modifications of the DLAS technique, adapted to particular applications. If the test molecule has sufficiently strong absorption lines, direct absorption measurements are used because the results of such measurements are relatively easy to interpret [1, 3]. In temperature measurements, one determines the absorption in lines differing in the position of the lower rovibrational level of a characteristic molecular species in the gas mixture. In the case of relatively slow processes and high concentrations, the medium can be thought to be at thermodynamic equilibrium, with a Boltzmann distribution of the level populations. The gas temperature can be determined either from the absorption amplitude ratio or, more accurately, from the ratio of the absorbances integrated over the entire linewidth. In the former case, the absorption can be monitored with the diode laser (DL) tuned to the peak absorption wavelength. This approach enables high-speed measurements, but it involves errors related to uncertainties in baseline determination [4, 5]. To obtain the integrated absorbance, one has to measure the line profile. To this end, the DL wavelength is scanned over a spectral range broader than the absorption linewidth, which enables more accurate baseline extrapolation but places limitations on the measurement speed [6].

In diagnostics of combustion processes in high-velocity flows, the temperature of the reacting mixture and the concentrations of its components must be measured under unsteady-state conditions. On the timescale of density and temperature variations in such flows (longer than 10^{-5} s), the medium can be thought to be at thermodynamic equilibrium, but the absorption must then be measured during a process time in the order of a fraction of a millisecond. Estimates indicate that, if the thickness of

M.A. Bolshov, Yu.A. Kuritsyn, V.V. Liger, V.R. Mironenko Institute of Spectroscopy, Russian Academy of Sciences, Fizicheskaya ul. 5, 142190 Troitsk, Moscow region, Russia;
e-mail: bolshov@isan.troitsk.ru, mironenko@isan.troitsk.ru;
S.B. Leonov, D.A. Yarantsev Institute of Thermophysics of Extreme States, Joint Institute for High Temperatures, Russian Academy of Sciences, Izhorskaya ul. 13/19, 125412 Moscow, Russia;
e-mail: s.leo@com.ru

Received 15 January 2009; revision received 28 April 2009
Kvantovaya Elektronika **39** (9) 869 – 878 (2009)
Translated by O.M. Tsarev

the combustion zone being probed is 1 – 10 cm, then at a pressure in the range 0.1 – 1 atm relative changes in probe beam intensity at a level $\Delta I/I_0 \sim 10^{-3}$ to 10^{-5} must be measured in $\sim 10^{-5}$ to 10^{-3} s. Another difficulty is that the active chemical reactions involved change not only the gas temperature but also the concentrations of the species participating in the combustion process and the gas mixture pressure. Pressure variations give rise to changes in test molecule absorption linewidth, which considerably complicates the algorithm for determining the sought gas parameters from the measured absorption signal.

One of the most important areas in experimental plasma aerodynamics [7] is the study of plasma-assisted combustion in high-velocity air flows. In nonpremixed fuel-oxidant flows (at velocities corresponding to Mach numbers $M \approx 2$), combustion is maintained by an additional electrical discharge which is initiated in the flow mixing zone. The discharge ensures high nonequilibrium concentrations of active radicals (OH and others) and accelerates the mixing process owing to the influence of spatial discharge inhomogeneities on the flow structure [8].

One way to assess the effectiveness of the discharge, which ignites and sustains the combustion process in high-velocity flows, is to monitor the temperature distribution in the ignition, combustion and flame zones and the distributions of the main combustion products at different stages of the process. In particular, the spatial distributions of water and carbon dioxide reflect fuel combustion dynamics and, eventually, the extent of the chemical reactions involved. Even though combustion processes in sub- and supersonic flows have been the subject of extensive theoretical and experimental studies, the effect of the spatiotemporal temperature and concentration profiles on the energy release processes in the reaction zone and hence on the engine efficiency has not yet been studied in sufficient detail. Acquiring reliable experimental data on the gas temperature and composition in different combustion zones continues to be a critical issue.

The short timescale of the processes involved (in the order of tenths of a millisecond), the spatial inhomogeneity of the medium and the inapplicability of measurement techniques that distort the flow impose stringent requirements on the measuring procedure and equipment.

The gas temperature and concentrations of molecular species in hot zones are often measured using coherent anti-Stokes Raman scattering (CARS) spectroscopy [9, 10]. This mature method provides accurate data on parameters of hot regions but requires expensive, complicated spectral and laser equipment and is difficult to apply in the diagnostics of real power units.

Techniques that utilise the emission spectra of characteristic molecules and radicals in the combustion zone have lower sensitivity because of the low population of the corresponding upper rovibrational levels. In this work, we use rovibrational levels with a frequency spacing of $\sim 7000\ \mathrm{cm}^{-1}$, and the mean gas temperature in the combustion zone is estimated at ~ 1000 K ($700\ \mathrm{cm}^{-1}$). Therefore, the upper and lower level populations are in the ratio $\mathrm{e}^{-10} \approx 4 \times 10^{-5}$. To assess the combustion efficiency, the gas temperature and concentration must also be measured downstream of the maximum energy release region, in zones where the gas temperature and hence the upper level population are still lower.

The approach best suited to such conditions is absorption measurements using tunable single-frequency DLs. Such sources offer high brightness, stable performance, and high spectral resolution without expensive or bulky spectral instruments.

The purpose of this work was to develop a DLAS procedure for water partial pressure and temperature measurements in the unsteady-state plasma-assisted combustion zone, with direct fuel injection into the supersonic air flow. Fuel combustion in this configuration is assisted by continuous discharge generation directly in the reaction zone. We designed an optical setup incorporating a laser module, control units, a DL beam delivery system, and a data acquisition and processing system. The procedure was tested using an experimental combustion chamber at the Joint Institute for High Temperatures (JIHT), Russian Academy of Sciences.

2. Basic relationships

When light propagates in an absorbing medium, its intensity, $I_{v,0}$, decreases according to the Bouguer – Lambert law. In the case of weak absorption and an isolated line, this law has the form

$$I_v = I_{v,0} \exp[-S(T)g(v - v_0)NL]$$

$$\approx I_{v,0} - I_{v,0}S(T)g(v - v_0)NL. \qquad (1)$$

Here, I_v is the transmitted intensity of the monochromatic light of frequency v (cm^{-1}) after it has traversed a distance L through the medium; $I_{v,0}$ is the intensity of the incident beam of frequency v; $S(T)$ is the line strength (integrated intensity); v_0 is the centre frequency of the absorption line; $g(v - v_0)$ is its lineshape function; and N is the concentration of the absorbing species. The line strength is a function of temperature, T. The lineshape depends on the gas temperature, pressure and composition and is determined by broadening mechanisms. At near-atmospheric pressures, the lineshape $g(v - v_0)$ is usually well represented by a Voigt function. In diagnostics of gas flows and flames, a typical full width at half maximum (FWHM) of absorption lines is $\sim 0.1\ \mathrm{cm}^{-1}$ (3 GHz). Therefore, the radiation from single-mode (single-frequency) DLs with linewidths in the range $\sim 10 - 50$ MHz can be considered monochromatic, and Eqn (1) ensures very good accuracy in interpreting absorption data.

The line strength as a function of temperature is given by

$$S(T) = S(T_0)\frac{Q(T_0)}{Q(T)}\exp\left[-\frac{hcE''}{k}\left(\frac{1}{T} - \frac{1}{T_0}\right)\right]$$

$$\times\left[\frac{1 - \exp(hcv/kT)}{1 - \exp(hcv/kT_0)}\right], \qquad (2)$$

where $Q(T)$ is the term in the partition function that depends only on temperature; and E'' is the energy of the lower quantum state involved in the transition.

If absorption is measured for several lines of the species of interest, the ratio of the strength between two of them is a single-valued function of temperature [we neglect the deviation of the last factor in (2) from unity]:

$$R = \left(\frac{S_1}{S_2}\right)_{T_0} \exp\left[-\frac{hc\Delta E}{k}\left(\frac{1}{T}-\frac{1}{T_0}\right)\right], \quad (3)$$

where S_1 and S_2 are the line strengths at temperature T_0, and ΔE is the difference in energy between the lower levels of the transitions responsible for the absorption. Thus, simultaneous absorption measurements for several lines can be used to determine the gas temperature in the probed volume, and the magnitude of absorption for a line with known spectroscopic parameters can be converted to the concentration of the absorbing species.

If the basic parameters of the medium have uniform longitudinal distributions, the temperature and concentration of absorbing species can be found easily from Eqns (1) and (3). In the case of nonuniform distributions, Eqns (1) and (3) provide the concentration and temperature averaged over the beam path. For many transitions of most simple molecules, the room-temperature line strengths have been accurately determined and can be found in databases (HITRAN [11], HITEMP, GEISA [12], SPECTRA [13]). The line strength at an arbitrary temperature, $S(T)$, can be evaluated by Eqn (2).

3. Experimental setup

3.1 Diode laser

We used a distributed feedback DL (NLK1E5GAA, NTT Electronics, Japan) emitting around 1.39 μm. The beam was outcoupled through a single-mode fibre pigtail. The temperature controller and current driver were Thorlabs TED350 and LDC202, respectively. When the temperature was varied from 5 to 49 °C, the total laser frequency tuning range at an injection current of 70 mA was 7199–7178 cm^{-1} (1.389082–1.393146 μm), i.e., $\Delta\nu/\Delta T \approx 0.48\ cm^{-1}\ K^{-1}$. Fast-speed laser frequency tuning was achieved by varying the injection current. The tuning range per scan depended on the injection current modulation frequency. At high frequencies, the range was markedly narrower. At a modulation frequency of 1 kHz and a laser temperature of 25 °C, varying the injection current in the range 10–120 mA ensured a frequency tuning range $\sim 1.2\ cm^{-1}$ in width, and the output power of the laser varied from 3 to 30 mW. Thus, for this type of DL, fast laser frequency modulation by the injection current entails considerable changes in beam intensity, i.e., strong amplitude modulation. This presented some difficulties in extracting parameters of the probed region from measurement results.

To calibrate the DL tuning range in absolute frequency, the absorption spectrum of water was measured at room temperature over the entire DL tuning range.* The observed lines were identified using HITRAN data [11]. In most of our experiments, the following absorption lines of H_2O were used: 7189.344 cm^{-1} ($E'' = 142\ cm^{-1}$), 7189.541 cm^{-1} ($E'' = 1255\ cm^{-1}$) and 7189.725 cm^{-1} ($E'' = 2005\ cm^{-1}$). These lines were selected because they differ considerably in the energy position of the lower level, which is of key importance in the temperature measurement procedure in question.

*We are grateful to Ya. Ponurovskii for his valuable assistance in the initial calibration of the DL and his insightful suggestions regarding how this type of laser should be operated.

The DL frequency was scanned by modulating the injection current with a sawtooth voltage from a laboratory-produced generator locked to the internal crystal oscillator of a storage oscilloscope.

3.2 Optical layout

In the first experiments on a pilot facility at JIHT, the DL beam was directed to the chamber across the laboratory's open space. The DL power supply units and data acquisition system were accommodated in the same room as the optical bench and discharge power supply. The main drawback to this arrangement was that the radiation was absorbed by the gaseous laboratory environment as it travelled from the optical system to the chamber (~ 2 m) and back. The absorption in air made a significant contribution to the signal, so that the signal due to the absorption in the test chamber could only be evaluated as the difference between two strong signals. Another significant drawback was the considerable level of electrical noise induced in the DL power supply by the discharge power supply. All this led us to change the initial experimental arrangement.

The final version is shown schematically in Fig. 1. The DL, power supply units, and data acquisition system were moved to another room (constrained by a dashed line in Fig. 1). The DL beam path through air was drastically reduced. To this end, the beam was delivered to the chamber through a 22-m-long single-mode fibre, the gradient-index collimator at the fibre output was placed right against the entrance window of the chamber, and the short-focus lens which focused the beam passed across the chamber into a photodetector was placed next to the exit window of the chamber.

To reduce the influence of amplitude modulation during DL frequency tuning and to extend the dynamic measurement range, we developed a differential measurement configuration with a reference channel. The output fibre of the laser (NTT Electronics, Japan) was connected to an fibre multiplexer (OOO Poisk-TR, Moscow), which coupled the DL beam into two fibres (1 : 1 intensity ratio). One fibre delivered the beam to the test chamber, and the other directly to the photodetector of the reference channel. In all the modules of the setup, single-mode glass fibres were used (9-μm core diameter and 125-μm cladding diameter). Both fibres had a gradient-index collimator at their output end, which produced a 1.8-mm-diameter beam with a divergence of $\sim 10^{-3}$ (the beam diameter increased to 5 mm over a distance of ~ 5 m).

The laser beam transmitted by the chamber was focused by a lens (5-mm focal length, 7-mm diameter) onto the surface of an InGaAs photodiode (Hamamatsu G8370-2) with an active area diameter of 2 mm. The photodetector was mounted in the immediate vicinity of the chamber, in a shielded case. The photodetector was situated next to the exit window of the chamber, so that the optical path length outside the chamber was less than 5 mm. In front of the detector was mounted an IKS-7 optical filter in order to eliminate the broadband intrinsic emission from the combustion zone. The passband of the filter was 0.9–2.6 μm, so that it cut off the visible, UV and mid-IR wavelengths. As a result, little or no intrinsic emission from the plasma reached the detector. A similar photodetector was used in the reference channel.

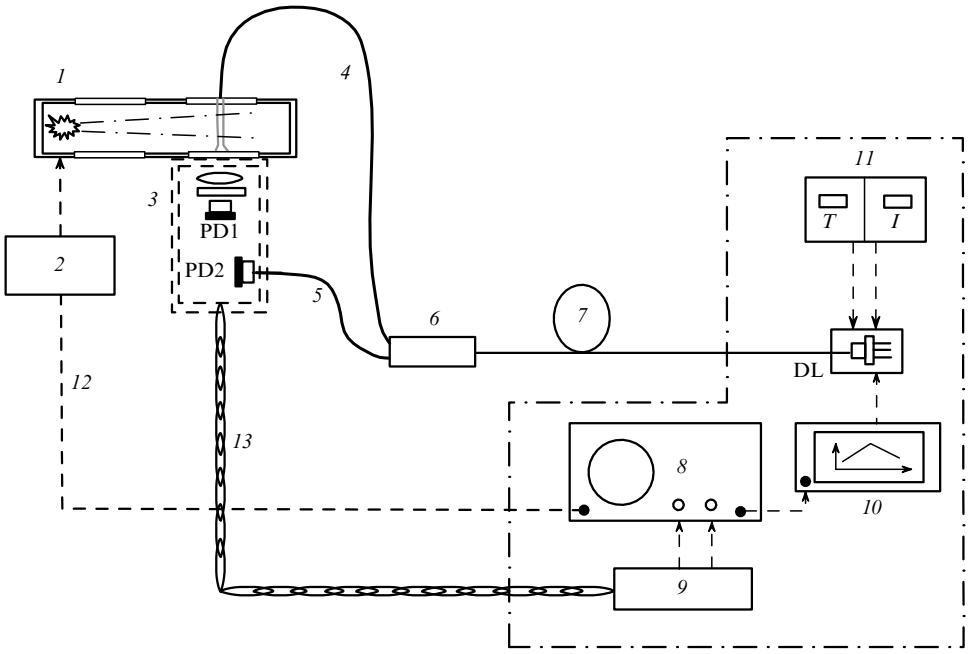

Figure 1. Schematic of the experimental setup: (*1*) test chamber enclosing the gas mixture flow; (*2*) gas inlet/discharge generation control system; (*3*) shielded module enclosing the preamplifier and photodetectors; (*4, 5*) single-mode fibre with a gradient-index collimator at its output end; (*6*) optical coupler; (*7*) single-mode fibre; (*8*) Agilent 54621A oscilloscope; (*9*) main amplifier; (*10*) sawtooth voltage generator; (*11*) DL controller; (*12*) synchronisation cable; (*13*) twisted pair.

3.3 Data acquisition system

The two photodetectors, lens, optical filters, and the input stages of the receiving circuit were housed in a casing with double electromagnetic shielding. The effective shielding of the photodetector and input preamplifier enabled the photodetector to be placed next to the chamber. The input preamplifier and photodiodes were powered by batteries isolated from ground. The output differential signal was fed through an $\sim$ 25-m-long shielded twisted pair to the main amplifier, accommodated in an adjacent room together with the DL drivers.

The differential measurement configuration takes advantage of the principle proposed by Hobbs [14]. The configuration is such that, in the absence of absorption in the chamber, the output signal is zero.

A simplified diagram of the input stage of the data acquisition system is shown in Fig. 2. The differential signal in this arrangement is the current at the node at the inverting input of the operational amplifier OA1. At this node, the oppositely directed photocurrents of the measurement and reference channels are summed. The photocurrent balancing element is the matched transistor pair MAT04, which is controlled by the feedback circuit through the base of one of the transistors so that the constant or slowly varying component of the differential photocurrent at the circuit output is zero. The differential measurement configuration ensures the maximum possible suppression of the DL beam intensity variations unrelated to the absorption by water molecules, including the amplitude modulation by the injection current, accompanying the DL frequency tuning,

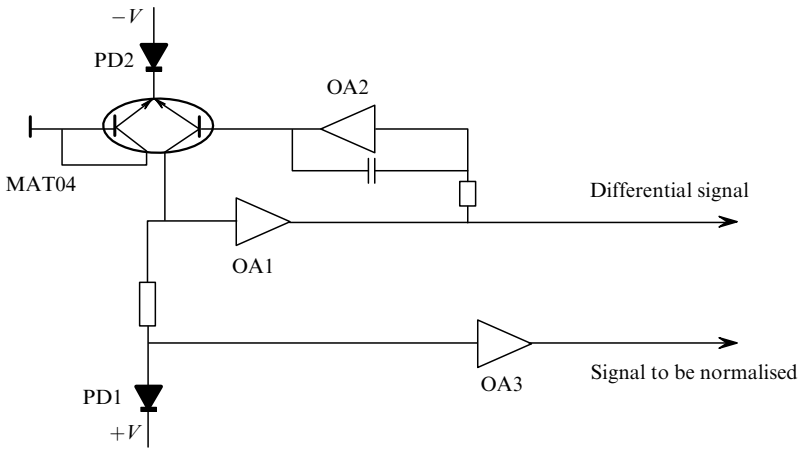

Figure 2. Diagram of the photodetector circuit: PD1 – photodetector of the absorption channel; PD2 – photodetector of the reference channel; OA – operational amplifier.

and the thermal fluctuations of the DL active area. The effectiveness of such suppression depends on the degree of identity between the characteristics of the measurement and reference channels, and may reach 40 dB at frequencies of up to several kilohertz without special adjustment.

The useful absorption signal emerges only in the measurement channel and, hence, it reaches the output of the differential amplifier OA1 without distortion. The absence of absorption in the reference channel is ensured by the design of the receiving unit, in which the fibre output end is located right against PD2.

To determine the absorption from the measured peak height by Eqn (1), a normalisation signal corresponding to the instantaneous photocurrent through the measurement channel is needed. The signal is developed across a resistor with a low nominal value, connected in series with the measuring photodiode PD1, and is then amplified by OA3.

The signals thus generated were then digitised for further processing on a computer. The photosignals were digitised on an Agilent 54621A two-channel oscilloscope. The differential absorption signal was fed to one input, and the normalisation signal, proportional to the instantaneous DL beam intensity, was fed to the other. The oscilloscope parameters are as follows: bandwidth, 60 MHz; sampling rate, 200 MHz; memory, 2 Mpts per channel. Because the baseline signal at the output of the differential amplifier was nearly zero, we were able to use inexpensive high-speed 8-bit analog-to-digital converters, which are widely used in digital oscilloscopes.

At the beginning of each measurement cycle, a drive pulse was fed to the gas flow/discharge/fuel injection control system [Fig. 1, module (*2*)]. The system generated a synchronising pulse that initiated the sweep in the storage oscilloscope, which in turn generated a synchronising pulse for the generator of sawtooth voltage for DL frequency scanning.

3.4 Test section of the IADT-50 facility

Our experiments were performed in the IADT-50 supersonic short-duration blowdown wind tunnel equipped with a closed test section [15]. Its length from the nozzle exit to the diffuser inlet is 600 mm, and its cross section varies from 60×72 mm at the entrance to 72×72 mm at the exit in the gas flow direction. The test section is equipped with three pairs of 100-mm-diameter optical windows equally spaced along its length. The main flow parameters under our measurement conditions are as follows: Mach number $M = 2$; static pressure $P = 150 - 300$ Torr; kinetic temperature, 300 K.

The results presented in this paper were obtained with the arrangement shown schematically in Fig. 3. An electrical discharge is generated on a flat ceramic wall between a set of electrodes arranged across the flow direction in an anode–cathode–anode configuration. The total discharge current I_d is 2–8 A and the deposited power W_d can be varied in the range 3–9 kW, which is within 5 % of the kinetic power of the air flow. The discharge leads to the formation of a downstream circulation zone [15], into which gas fuel (hydrogen in this study) is injected. To compensate the combustion-induced pressure rise and prevent thermal blocking, the tunnel area increases downstream of the discharge/fuel injection zone. The test time is 0.5 s. The discharge is initiated after the flow reaches a quasi-steady state, and is maintained for 80–100 ms. Fuel is injected starting at 20–30 ms after the discharge onset and until 20–30 ms after termination of the discharge. Note that combustion ceases at the instant when the discharge is switched off.

In the described experiments, DLAS measurements were taken in the hot wake region downstream of the blowdown tunnel expansion (5 mm from the wall). We varied the fuel mass flow rate and discharge characteristics.

4. Results and discussion

4.1 Primary processing of transient absorption data

Using the setup described above, we performed measurements with hydrogen and ethylene as fuels at various gas jet parameters and fuel flow rates. Here, only the measurement results obtained for hydrogen as fuel are presented. Note that, under all the conditions described in this paper, the water concentration was high enough for direct absorption to be measured.

The experimental results obtained in one test run have the form of two one-dimensional (1D) data files, each consisting of 2×10^6 data points. One file is the result of ~ 600 scans of the differential signal, and the other is obtained by simultaneously measuring the instantaneous DL beam intensity. The total measurement time is 500 ms.

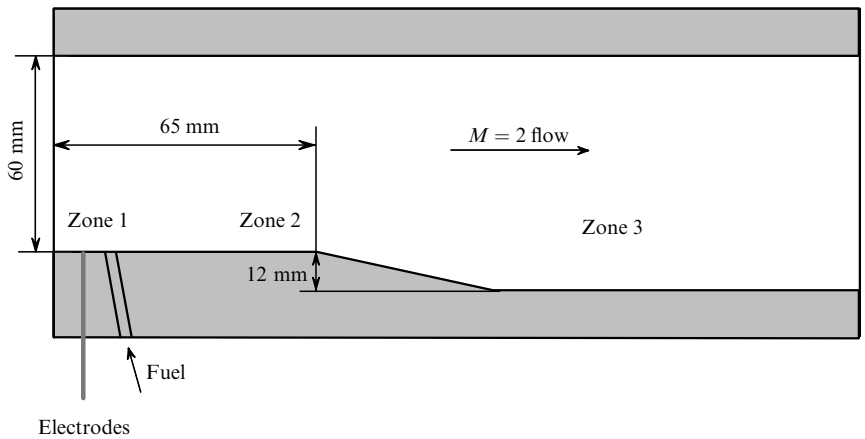

Figure 3. Test section configuration: (*1*) discharge-fuel interaction zone; (*2*) combustion zone; (*3*) flame zone and hot wake region.

As an example, Fig. 4 presents data obtained in one test run. The test parameters were as follows: static pressure in the test section, 130 Torr; hydrogen mass flow rate, 0.5 g s^{-1}.

In Fig. 4a, one can see characteristic points in time. The air inlet valves were opened 30 ms after the beginning of the test run, and 20 ms thereafter the flow in the tunnel reached a supersonic velocity ($M = 2$). After 120 ms, an electrical discharge was initiated. Next, fuel was injected into the test section, and combustion began. Figure 4b presents a small portion of the differential signal trace, covering three DL scans, i.e., approximately 2.5 ms. This portion is situated near the midpoint of the combustion range. Figure 4c shows the time dependence of the DL beam intensity, which varies in a sawtooth-like fashion in response to the injection current modulation. This dependence was used to evaluate the temperature and water concentration from spectral data.

The time trace in Fig. 4a was first converted to a 2D image, which considerably simplified initial analysis of the measured signal and enabled rapid identification of the main stages in the combustion process. Subsequently, we focused on the most characteristic time intervals, containing important information about the development of the combustion process. The digital image processing technique we used is based on an open source code [16]. It enables visualisation of experimental data immediately after acquisition and a marked reduction in data processing time.

Figure 5 presents the results obtained by processing the data displayed in Fig. 4a. Figure 5a shows a 2D image of the process, and Fig. 5b shows the corresponding absorption spectra around 7189 cm^{-1}. The image in Fig. 5a was derived from sequential experimental scans in the test run in question. All the scans were within the most important time span: the first 250 ms of the process. This time span includes the mixing of the air and fuel flows, ignition, gas-mixture combustion, termination of the combustion process and cooling. In each scan, the DL frequency v is varied from left to right within the range chosen: the frequency first decreases with increasing injection current and then increases on the other side of the sawtooth. All the scans are arranged sequentially, under one another. Thus, in this image the magnitude of the signal, F, in pixel (x, y) represents the intensity of the beam transmitted through the chamber, I, at time t:

$$F(x, y) = I(v(t), n(t)).$$

In the system of coordinates we use, the origin is in the top left corner of the image. The x axis is directed to the right and represents the variation in frequency in the scan. The y axis is directed downwards and represents the scan number n, corresponding to the time elapsed after the beginning of the test run ($t = 0$). The data thus represented have the form of a 2D image illustrating the time evolution of the absorption spectrum of the probed region. Absorption was measured in a spectral range ~ 1 cm^{-1} in width (x axis), one scan took ~ 830 μs, and the total measurement time

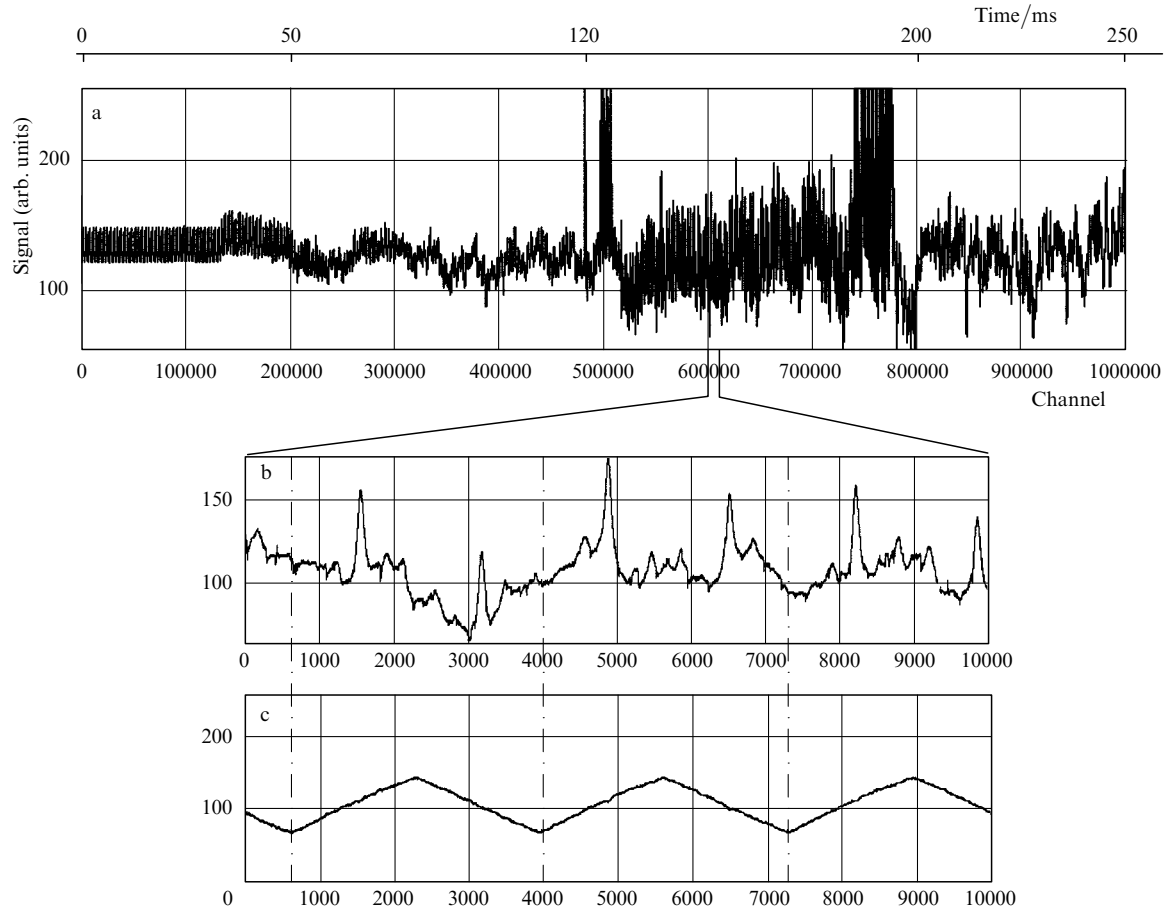

Figure 4. (a) Oscilloscope trace of the differential signal during the first 250 ms of a test run; (b) portion of the trace covering three DL scans; (c) corresponding sawtooth variation in DL beam intensity.

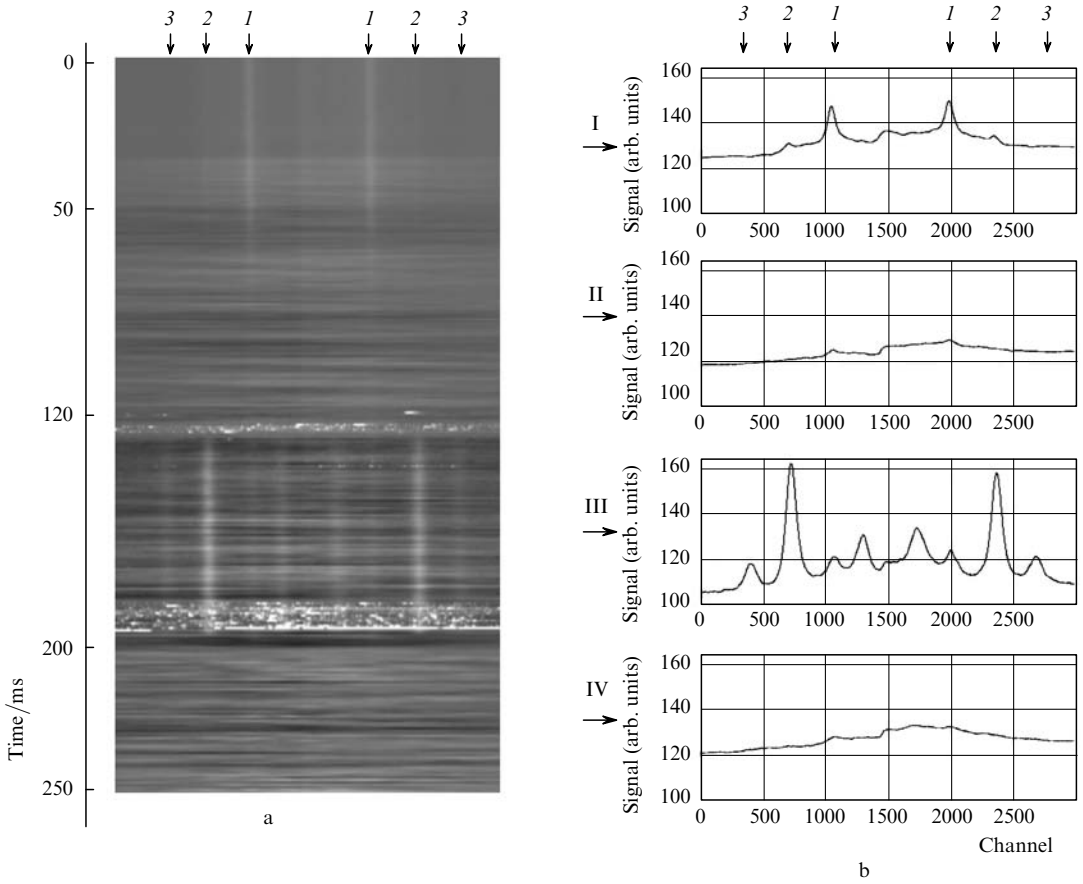

Figure 5. Example illustrating the data processing procedure (data displayed in Fig. 4). (a) 2D image of the scans obtained during the first 250 ms; (b) absorption spectra of H_2O averaged over 60 scans at different stages (I – IV) of the combustion process. The time axis is the same as in Fig. 4. The arrows under italicised numbers show the positions of the absorption lines used in subsequent data processing: (*1*) 7189.344, (*2*) 7189.541 and (*3*) 7189.715 cm^{-1}.

was 250 ms (y axis). The program allows one to specify any number of scans for processing and enables dynamic averaging over any time span.

The spectra displayed in Fig. 5b were obtained as averages over 60 scans within four characteristic time intervals. The scan reversal point is located near the midpoint of the horizontal scale. In stage I, the chamber is filled with air at a pressure of ~ 120 Torr. Both the 2D image and the corresponding spectrum show a well-defined 'cold' line at 7189.344 cm^{-1}. At the end of stage I, about 50 ms after the beginning of the process, the flow in the tunnel reaches a supersonic velocity. The static gas temperature T is then ~ 200 K, i.e., well below room temperature. This leads to water vapour freeze-out. As a result, approximately 20 – 30 ms after the beginning of the test, the absorption lines of water weaken and disappear, which is well seen in both the 2D image and the spectrum corresponding to stage II. After ~ 120 ms, a discharge is initiated, and 20 ms thereafter fuel injection begins. At this point in time, combustion develops, accompanied by a rapid rise in temperature, and water vapour appears in the combustion zone. In Fig. 5, one can see well-defined 'hot' absorption lines of water at 7189.715, 7189.541 and 7189.199 cm^{-1}. At the same time, the 'cold' line (7189.344 cm^{-1}) becomes substantially weaker. This type of spectrum persists throughout the combustion process (about 50 ms). Next, the combustion process ceases (IV) and the temperature of the supersonic flow drops rapidly, leading to water vapour freeze-out and causing almost all of the absorption lines of H_2O to disappear, as clearly evidenced by Fig. 5a (after ~ 200 ms).

4.2 Evaluation of combustion parameters

The simplest algorithm for extracting information about temperature is evaluation of T from the intensity ratio of two well-resolved absorption lines by Eqn (3). The intensity ratio is independent of the gas pressure and, hence, of the absorption linewidths. In this approach, however, an important point is to accurately determine the baseline, which is needed to calculate the integrated intensity of the lines in the measured spectrum. Considerable uncertainties in baseline position give rise to large errors in the integrated intensity of the absorption line. This is particularly important in the case of baseline fluctuations in the DL wavelength tuning range.

We used an alternative approach: the spectrum measured in the scanning range was fitted with a spectrum simulated using data bases.

The combustion zone parameters were extracted from the differential signal obtained in individual scans or by summing up several scans. Prior to analysis of spectra, we performed low-frequency digital filtration of the data set.

In all our experiments, the absorption was weak, so that relation (1) was fulfilled. Under such conditions, the differential signal Y_i at frequency v_i can be represented in the form

$$Y_i = \alpha I_{0,i} \sum_i S_j(T) g_j(v_i - v_{0,j}) NL + b_i + \varepsilon_i, \quad (4)$$

where α is the gain of the recording electronics; $I_{0,i}$ is the DL beam intensity at frequency v_i; $v_{0,j}$ is the centre frequency of line j; the term b_i represents the baseline; and ε_i is the residual (difference) between the experimental and simulated spectra. The other parameters were introduced in Eqn (1).

To fit experimental data with an analytical function, we determined parameters (instantaneous DL frequency, gas temperature, gas pressure, and baseline parameters) that minimised the rms deviation. Line strengths were evaluated by Eqn (2) using the $S(T_0)$ values for $T_0 = 296$ K and the lower level energies from the HITRAN database [11]. The partition function $Q(T)$ was determined using SPECTRA data [13]. The lineshape $g_i(v_i - v_{0,i})$ was represented by a Voigt function. In the first step of $g_i(v_i - v_{0,i})$ calculation, only the line broadening by air was taken into account.

The baseline b_i in (4) was fitted by polynomials of the form $b_i = \sum k_n Q_{in}$, where k_n are fitting parameters and Q_{in} are orthogonal polynomials. We used polynomials of degree no higher than two.

In the first step, the simulated spectrum was fitted to the observed frequency response using the peak positions of the absorption lines selected for determining the temperature. DL frequency tuning during a scan was taken to be linear in time. In the next step, physically meaningful initial values of the gas temperature and pressure were selected, and the fitting parameters that minimised the mean-square deviation in (4) were found by linear least squares regression. Subsequently, a nonlinear least squares iteration procedure (Nedler–Mead simplex routine [17]) was used to fit the frequency scale, temperature, and pressure.

The extraction of probed-zone parameters is illustrated below by the example of the data obtained under the following conditions: hydrogen mass flow rate $G = 0.5$ g s^{-1}; static pressure in the test section upstream of the combustion zone, 130 Torr. Figure 6 shows the measured spectrum of two hot lines obtained as the average over 30 scans in the range 140–165 ms after the beginning of the process and the best fit spectrum. As seen, the measured spectrum is well represented by model (4): the rms deviation $\sqrt{\langle \varepsilon_i^2 \rangle}$ is ~ 0.4 %. An important point related to fitting absorption lines with a Voigt function is worth noting. It is known that, when lineshapes are fitted with a Voigt function, the Lorentzian and Doppler broadening contributions are difficult to separate. At the same time, when two absorption lines differing in lower level energy are used in fitting, the temperature and, hence, the Doppler contribution can be determined from the ratio of their integrated intensities, and unfolding the Voigt lineshape is no longer an ill-posed problem.

The above fitting procedure yields the parameters of interest: the temperature of the probed zone, the total gas pressure and the corresponding absorption spectrum. The concentration of water molecules was determined using the experimentally determined absorption, $\Delta I/I_0$, and the distance between the windows across the chamber, L. In the test run under consideration, the absorption in the stronger line was ~ 2 %, and that in the weaker line was about 0.5%. Note that, at $T = 1000$ K, a 1 % uncertainty (5×10^{-5}times the total intensity) in the intensity of the weaker line leads to an about 10 K uncertainty in temperature.

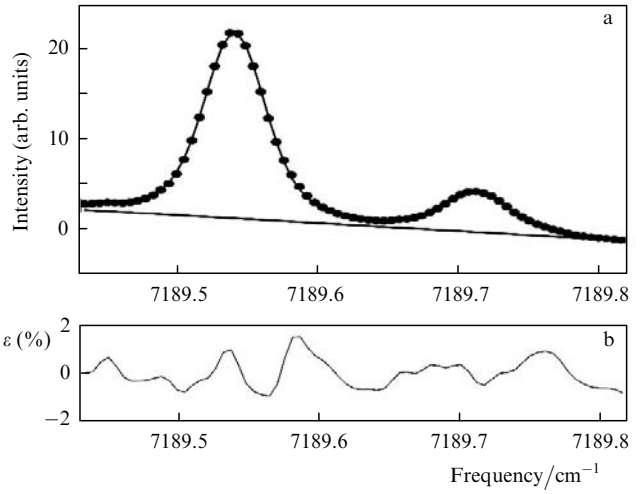

Figure 6. (a) Measured (filled circles) and simulated (solid line) absorption spectra; the inclined line is the best fit baseline (straight-line fitting). (b) Difference between the spectra, ε, expressed as a percent of the maximum intensity.

In the test run represented in Fig. 6, the time-averaged gas temperature in the probed zone and H_2O partial pressure evaluated from the concentration of water molecules were 1050 K and 21 Torr, respectively.

The total gas pressure in the probed zone was initially estimated at 350 Torr, but at that stage only the air pressure broadening of the water lines was taken into account in the fitting procedure. In effect, a significant contribution comes from water self-broadening. According to HITRAN data [11], the self-broadening coefficient for the lines under consideration is a factor of 5–6 greater than the air pressure broadening coefficient. Therefore, the above estimate of the total gas pressure is too high. To more accurately determine the gas pressure, the broadening coefficient for the water lines was corrected using the self-broadening coefficient from [11] and the fitted value of water concentration. As a result, the total gas pressure in the probed zone was determined to be 200 Torr, in good agreement with that measured independently by static pressure transducers.

The accuracy of the calculation procedure was checked using an absorption spectrum measured in the test chamber at an air pressure of 120 Torr. The temperature thus determined was 19 °C, in good agreement with the ambient temperature in the room.

The spectrum in Fig. 6 was obtained as the average over 30 scans. The fairly large signal-to-noise ratio in our measurements allows data processing with a smaller number of scans, giving the time dependence of the gas temperature. Figure 7 illustrates the variation of the gas temperature in the combustion zone during the same test run as above, assessed by processing a larger number of scans (64) in a wider time interval (130–185 ms). The data points were obtained as moving averages over nine scans, while uniformly increasing the number of the first scan. The filled circles represent the data obtained by processing the first half of the scan (decreasing DL frequency), and the open circles represent the second half of the scan (increasing DL frequency). The solid line shows the average of the two halves. Note good agreement between the temperatures evaluated from the rising- and decreasing-frequency portions of the scans (T_i^+ and T_i^-, respectively).

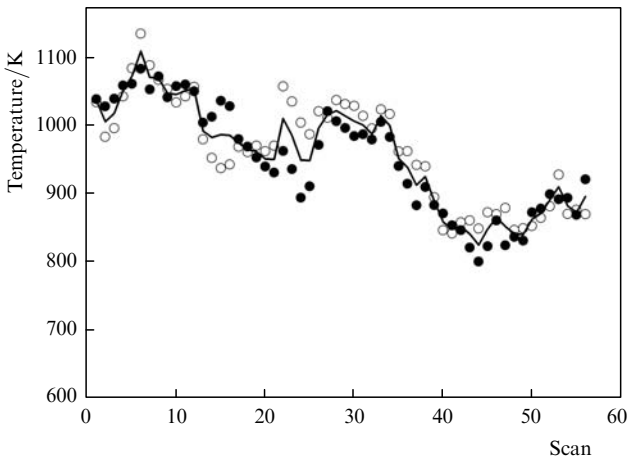

Figure 7. Time variation of the gas temperature in the probed zone. The first scan was made 130 ms after the beginning of the test rum. The scan time is 830 μs.

These data were used to estimate the accuracy in our temperature measurements. The gas temperature in the probed zone was assumed to be constant during a given scan (830 μs). Each $T_i^{+,-}$ value is determined with a random error $\varepsilon_i^{+,-}$. The temperature difference $\Delta T_i = (T_i^+ - T_i^-)$ is equal to $\varepsilon_i^+ - \varepsilon_i^-$. Assuming the $\varepsilon_i^{+,-}$ values to be statistically independent and to have the same variance σ^2, we obtain the following estimate of the mean-square deviation in temperature:

$$\sigma^2 = \sum_i^m (T_i^+ - T_i^-)^2/2m, \tag{5}$$

where m is the number of spectra used in data processing. In this way, the accuracy (statistical error) in our temperature measurements was estimated at $\sigma = 40$ K. Note that the results obtained by the described procedure are also affected by systematic errors in the spectroscopic parameters taken from databases. Analysis of the literature allows such errors to be estimated at a few percent.

5. Conclusions

We developed a procedure for remote temperature and water vapour concentration measurements using tunable DL absorption spectroscopy. The procedure utilises absorption lines that differ considerably in the energy of the lower level of the rovibrational transition responsible for the absorption, so that temperature changes are accompanied by changes in the relative intensities of the lines. To measure absorption spectra, the DL frequency is scanned in a sawtooth-like fashion around 7189 cm^{-1} at a frequency of ~ 1 kHz. The scan range is ~ 1 cm^{-1} in width. In this range, we measure the absorption lines of H_2O at 7189.344 cm^{-1} ($E'' = 142$ cm^{-1}), 7189.541 cm^{-1} ($E'' = 1255$ cm^{-1}) and 7189.715 cm^{-1} ($E'' = 2005$ cm^{-1}). The procedure enables spectra to be measured with a time resolution of ~ 1 ms, offering the possibility to probe transient processes in remote systems.

In data processing, we used 2D representation illustrating the dynamics of the absorption spectrum. The gas temperature and water vapour concentration were determined by fitting the measured spectrum with a spectrum calculated using the spectroscopic parameters taken from the HITRAN and SPECTRA databases. The adjustable parameters were the gas temperature, total gas pressure and baseline level.

The described procedure was used to assess parameters of electrical-discharge-assisted supersonic combustion in the IADT-50 blowdown wind tunnel (JIHT). We determined the combustion-time-averaged gas temperature and water vapour partial pressure in the hot wake region: 1050 K and 21 Torr, respectively. This allowed us to evaluate for the first time the local fuel-air equivalence ratio in the unsteady-state combustion zone of the IADT-50 and the combustion efficiency in the zone adjacent to the discharge-fuel interaction region: $ER \approx 0.15$ (at a mass flow rate $G = 0.25$ g s^{-1}) and $\eta > 0.9$, respectively. These ER and η values reflect the effectiveness of the proposed configuration for gas fuel combustion stabilisation in high-velocity air flows. The use of an electrical discharge in the test section for promoting the combustion process extends the concentration range of stable reactions towards lean mixtures ($ER \sim 0.15$), maintaining high combustion efficiency ($\eta > 0.9$).

The fairly large signal-to-noise ratio in our measurements allowed us to assess the dynamics of the gas temperature during the combustion stage ($\Delta t = 50$ ms). The estimated accuracy in our temperature measurements in the probed zone was $\Delta T \sim \pm 40$ K. Future work will concentrate on the effect of the temperature of the main flow and the nature of the fuel on the temporal parameters and spatial profiles of different combustion zones. In addition, we will examine various geometric configurations of the test section in the discharge-fuel interaction region.

Acknowledgements. This work was supported by the Physical Sciences Division of the Russian Academy of Sciences (basic research programme Optical Spectroscopy and Frequency Standards, OFN-10, Project No. 4.6) and the Presidium of the Russian Academy of Sciences (programme No. 9: Characterisation of Matter under Extreme Conditions; section 9.2: Fundamental Issues in Magnetoplasma Aerodynamics).

References

1. Allen M.G. *Meas. Sci. Technol.*, **9**, 545 (1998).
2. Sanders S.T., Mattison D.W., et al. *Opt. Express*, **10**, 505 (2002).
3. Richter D., Lancaster D.G., Tittel F.K. *Appl. Opt.*, **39**, 4444 (2000).
4. Baer D.S., Nagali V., Furlong E.R., Hanson R.K., Newfield M.E. *AIAA J.*, **34**, 489 (1996).
5. Sanders S.T., Baldwin J.A., Jenkins T.P., et al. *Proc. Combust. Inst.*, **28**, 587 (2000).
6. Zhou X., Liu X., Jeffries J.B., Hanson R.K. *Meas. Sci. Technol.*, **14**, 1459 (2003).
7. *Proc. 1–7th Intern. Workshop «Magneto-Plasma Aerodynamics in Aerospace Applications»* (M.: IVTAN, 1999–2007).
8. Leonov S.B., Yarantsev D.A., Napartovich A.P., Kochetov I.V. *IEEE Trans. Plasma Sci.*, **34**, 2514 (2006).
9. Greenhalgh D.A., in *Advances in Non-Linear Spectroscopy*. Clark R.J.H., Hester R.E. (eds) (New York: Wiley, 1988) p. 193.
10. Eckbreth A.C. *Laser Diagnostics for Combustion Temperature and Species* (Amsterdam: Gordon and Breach, 1996).
11. Rothman L.S. Jacquemart D., Barbe A., et al. *J. Quant. Spectrosc. Radiat. Transfer.*, **96**, 139 (2005); HITRAN website: http://www.hitran.com/.

12. Jacquinet-Husson N., Scott N.A., Chedin A., et al. *J. Quant. Spectrosc. Radiat. Transfer.,* **109**, 1043 (2008); GEISA website: http://ara.lmd.polytechnique.fr/.
13. SPECTRA Information System; website: http://spectra.iao.ru.
14. Hobbs P.C.D. *Appl. Opt*., **36**, 904 (1997).
15. Leonov S.B., Yarantsev D.A. *Mekh. Zhidk. Gaza*, **6**, 121 (2008).
16. Abramoff M.D., Magelhaes P.J., Ram S.J. *Biophotonics Int*., **11** (7), 36 (2004); ImageJ website: http://rsb.info.nih.gov/ij/.
17. Nelder J.A., Mead R. *Comput. J*., **7**, 308 (1965).